Multi-Objective Scale Independent Optimization of 3-RPR Parallel Mechanisms

M. H. Saadatzi * K.N. Toosi University Tehran, Iran

M. Tale Masouleh † Laval University Québec, Canada

H. D. Taghirad‡ K.N. Toosi University Tehran, Iran

C. Gosselin § Laval University Québec, Canada

M. Teshnehlab ¶ K.N. Toosi University Tehran, Iran

Abstract—*This paper deals with the optimization of 3-RPR planar parallel mechanisms based on different performance indices including kinematic sensitivity, stiffness, workspace and singularity. The optimization is implemented in sequence using first a single objective technique, differential evolution, and then resorting to a multi-objective optimization concept, the so-called nondominated sorting genetic algorithm-II. The results revealed that the optimality of the mechanism under study is scale-independent for the considered optimization objectives. Moreover, based on the scale invariance property of the main objectives, it follows that different kinetoestatic objective functions must be scale invariant. The relations for the kinetoestatic objective expressions as functions of mechanism scale are derived and to circumvent the problem of unit inconsistency the rotational and translational parts of these objectives are considered separately. To overcome the problem of inconsistent objectives in optimization algorithm, a Pareto-based multi-objective approach is used which preserves the scale invariance property.*

Keywords: Parallel mechanism, Scale-invariant mechanism performance indices, Kinematic sensitivity, Rotational and translational stiffness, Multi objective optimization, Differential evolution, NSGA-II.

I. Introduction

The last two decades have witnessed an important spread in the use of parallel mechanisms in applications such as motion simulators, machine tools and even nano-manipulators. Parallel mechanisms have evolved from rather marginal devices. They are becoming the state of the art in the commercial world due to their high quality in some kinematic properties, such as accuracy, although their workspace is more constrained than their counterpart, serial mechanisms.

Therefore, in order to displace the serial mechanisms in some particular applications, the optimal design of parallel mechanisms has received special attention in order to alleviate some of their shortcomings in terms of kinematic properties, such as limited workspace and complex singularities. This is exemplified by a large increase in the number of papers published on the *singularity-free workspace* of parallel mechanisms.

For a long time, the synthesis of parallel mechanisms for a given motion pattern has been carried out mainly using intuition and ingenuity. The recent development of a systematic approach for the *type synthesis* of parallel mechanisms has provided insight into the classification of a large number of parallel mechanisms based on their motion pattern [1]. This is the first step toward designing a parallel mechanism which consists in selecting the architecture which makes the most sense from the manufacturing, motion pattern, assembly, workspace and stability perspectives. The second step is to analyse the kinematic properties, such Inverse and Forward Kinematic Problem (IKP and FKP), workspace and singularity. The third step is to refine these kinematic properties by selecting a set of criteria to ascertain that the parallel mechanism under study reaches the required performance for a given task, the central subject of this paper.

The performances of parallel mechanisms are highly dependent on their geometric properties. Numerous examples show that a careful design optimization can lead to significant improvements over the initial design [2]. In practice, there are always multiple performance requirements to be satisfied. Usually, for each requirement an index is defined which indicates to what extent the requirement is satisfied or violated [2].

Numerous performance indices have been proposed to compare robot architectures based on their kinematic properties. The most notorious kinematic indices, which are manipulability and dexterity, still entail some drawbacks [2–4], which are mainly due to problems which prevent the definition of a single invariant metric for the special Euclidean group. Recently, in [3], two distinct metrics were defined and formulated, namely the maximum rotation sensitivity and the maximum point-displacement sensitivity. These two indices provide tight upper bounds to the end-effector rotation and point-displacement sensitivity under a unit-magnitude array of actuated-joint displacements. Moreover, from a statics stand point, stiffness stands for the ability of a body or structure to resist the deformations due to the action of external forces. Usually, the sum of the diagonal elements of the stiffness matrix is used as the system stiffness performance index, which suffers from the unit inconsistency [5].

Independent investigation of different performance in-

*saadatzi@ee.kntu.ac.ir
†mehdi.tale-masouleh.1@ulaval.ca
‡Taghirad@kntu.ac.ir
§Clement.Gosselin@gmc.ulaval.ca
¶Teshnehlab@eetd.kntu.ac.ir

dices which can be achieved by resorting to single objective optimization is helpful to have a better understanding of their effects on the mechanism performance. In this paper, Differential Evolution (DE) [6,7] is proposed , which in comparison with other Evolutionary Algorithms (EA), such as genetic algorithms and evolutionary strategy [8], differs significantly in the sense that distance and direction information from the current population are used to guide the search process. Moreover, the original DE strategies were developed to be applied to continuously-valued landscapes.

Once the optimum value of one objective is obtained, the corresponding optimum values of the design parameters usually yield unsatisfactory results for the other objectives. For instance, as it was revealed in [2], the SSM, a simplified Gough-Stwerat platform, with maximal workspace volume for a given stroke of the actuators has similar base and moving platform and is therefore architecturally singular. In the case that more than one performance objective should be considered, a graphical approach based on an atlas representation of performance indices would be really helpful. However, this approach may be useful only for a very small set of design parameters.

Based on the methodology proposed in the literature, when numerous performance objectives are in place the problem can be made equivalent to a single objective optimization by combining them in a weighted linear sum. Clearly, the solution obtained will depend on the relative values of the specified weights and hence a priori information on the problem is needed. Another drawback with this method is that the sum of different objectives with inconsistent units may result in a meaningless concept for the problem and therefore lead to erroneous conclusions.

The objective way of solving multi-objective problems requires a *Pareto-compliant ranking* method [9], favouring non-dominated solutions. Here, no weight is required and thus Pareto solutions are those for which improvement in one objective can only occur with the worsening of at least one other objective. Thus, instead of a unique solution to the problem, the solution to a multi-objective problem is a set of Pareto points. Among this points the designer should choose those which tend to fit closely with the specific design objective. In this paper, the Nondominated Sorting Genetic Algorithm-II (NSGA-II) [10] which is a standard Pareto-based multi objective approach is used.

Defining a set of comprehensive and practical objectives which covers all kinematic properties, such as singularity-free workspace and mechanical interferences, is a delicate task. Hence, before using intelligent methods the mechanism must be investigated completely, workspace and singularities of the mechanism should be analysed and proper constraints must be devised. Upon this investigation, intelligent methods can be used to specify the remaining parameter selection freedom of design process. Using intelligent methods solely, would result in a lengthy computation process, and most of the times the designs obtained suffer from singularities and mechanical interferences, therefore the designs are practically incompetent.

This paper aims at developing a general methodology for the optimization of parallel mechanisms, as a follow up of the study conducted in [3, 11], and the 3-RPR parallel mechanism is considered as a case study for this purpose. The remainder of this paper is organized as follows. First the geometric modeling and the first-order kinematic analysis, Jacobian matrix, of 3-RPR parallel mechanisms are reviewed. Then the constant-orientation workspace and singularity configurations of a scaled 3-RPR parallel mechanism are investigated and extended to the unitary mechanism. The paper pursues the study by illustrating different kinetostatic performance indices and their relations to the scaled mechanism. The single and multi-objective optimization procedure is elaborated where the emphasis is placed on refining the objective parameters to be suitable to be implemented in the optimization procedure. The single objective procedure is applied by resorting to the DE concept in order to lay down the essentials for the multi-objective optimization. Subsequently, Pareto-based multi-objective optimization is considered and NSGA-II is used to design the optimal mechanism. Finally, the paper concludes with some remarks that provide insight into ongoing works for extending this study to other types of parallel mechanisms.

II. Architecture and First-order Kinematic Review of 3-RPR Parallel Mechanism

A. Architecture Review

Figure 1 illustrates the schematic representation of a 3-RPR parallel mechanism. As depicted in Fig. 1, a planar 3-RPR parallel mechanism with actuated prismatic joints consists of a fixed triangle base $\triangle A_1A_2A_3$ and a mobile triangle platform $\triangle B_1B_2B_3$. The passive revolute joints, with coordinates A_i and B_i, are connected by the prismatic actuator of variable length ρ_i, $i = 1, 2, 3$, where the unit vector along the prismatic direction is denoted by $\mathbf{n}_i = [n_{i_x}, n_{i_y}]^T$. The pose (position and orientation) of the mobile platform is described by two coordinate systems as shown in Fig. 1. A reference frame O_{xy} is attached to the base by selecting $A_1 \equiv O$ as the origin. The mobile frame $O'_{x'y'}$ is attached to the platform by selecting a given point on the mobile platform, $C \equiv O'$, as the origin. The position of the mobile platform, coordinates of C, with respect to the fixed frame, is represented by $\mathbf{p} = [x, y]^T$. The position vector of point B_i in the fixed and mobile frame is denoted respectively by vector $\mathbf{b}_i$ and $\mathbf{b}'_i$, $i = 1, 2, 3$. It should be noted that in this paper the superscript $'$ for a vector stands for a representation in the mobile frame $O'_{x'y'}$. Finally, vector connecting B_i to C expressed in the fixed frame is represented by $\mathbf{s}_i$. The rotation matrix, $\mathbf{Q}$, representing the

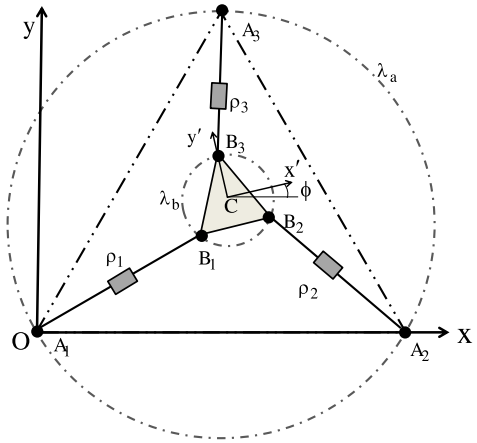

Fig. 1. Schematic representation of a 3-RPR parallel mechanism.

rotation of the platform from frame O_{xy} to frame $O'_{x'y'}$ is:

$$\mathbf{Q} = \begin{bmatrix} \cos\phi & -\sin\phi \\ \sin\phi & \cos\phi \end{bmatrix} \tag{1}$$

where ϕ stands for the rotation angle of the platform around the axis perpendicular to the plane of the mobile platform.

B. First-order Kinematics and Jacobian Matrix

The IKP, FKP, and Jacobian matrix of a 3-RPR parallel mechanism has been extensively studied [2]. The first-order kinematic expression for the i^{th} limb can be written as:

$$\dot{\rho}_i = \mathbf{n}_i \cdot \dot{\mathbf{p}} + (\mathbf{s}_i \times \mathbf{n}_i) \cdot \mathbf{\Omega} \tag{2}$$

where $\dot{\mathbf{p}} = [\dot{x},\, \dot{y}]^T$ is the rate change of the position of point C with respect to time and $\mathbf{\Omega} = [0,\, 0,\, \omega]^T$ is the angular velocity. Hence, the first-order kinematics of the mechanism may be rewritten in terms of dimensionally homogeneous arrays for the unit mechanism:

$$\dot{\boldsymbol{\rho}} = \mathbf{J}_r \omega + \mathbf{J}_p \dot{\mathbf{p}} \tag{3}$$

where

$$\mathbf{J}_p = \begin{bmatrix} \mathbf{n}_1^T \\ \mathbf{n}_2^T \\ \mathbf{n}_3^T \end{bmatrix}, \qquad \mathbf{J}_r = \begin{bmatrix} J_{r1} \\ J_{r2} \\ J_{r3} \end{bmatrix} \tag{4}$$

In the above, $\dot{\boldsymbol{\rho}} = [\dot{\rho}_1,\, \dot{\rho}_2,\, \dot{\rho}_3]^T$ and:

$$J_{ri} = (\mathbf{s}_i \times \mathbf{n}_i) \cdot \mathbf{k}, \quad i = 1, 2, 3 \tag{5}$$

where $\mathbf{k}$ stands for the unit vector along the axis perpendicular to the plane of the mobile platform. The lines of $\mathbf{J}_p$ are unit vectors, meaning that it is unaffected by the overall scale of the mechanism. Emerging here is the notion of *scale* of the mechanism and here and, throughout this paper, its factor is denoted by l. However, $\mathbf{J_r}$ cannot be considered as scale-independent due to the presence of the non-unite vector $\mathbf{s}_i$. Thus the scale factor appears in $\mathbf{J}_r$ and upon considering $\mathbf{J} = [\mathbf{J}_p\, \mathbf{J}_r]^T$, one has: $\mathbf{J} = [\mathbf{J}_p\ \mathbf{J}_{r0}]^T$ where $\mathbf{J}_{r0} = \frac{1}{l}\mathbf{J}_r$. A scaled Jacobian can then be defined as $\mathbf{J}_s = [\mathbf{J}_p\ \mathbf{J}_{r0}]$.

III. Preliminary Investigation for the Dimensional Synthesis of 3-RPR Parallel Mechanisms

The dimensional synthesis of mechanical systems, including parallel mechanisms, pertains to determining the dimensions of the mechanism in such a way that it complies as closely as possible to the performance needed for the required task. In what follows, some kinematic properties of the 3-RPR parallel mechanisms, constant-orientation workspace and singularities, are reviewed and their scalability is examined. The discussion is based on the results presented in [11–13] which leads to gain insight into an appropriate initial design of 3-RPR parallel mechanisms for launching the optimization procedure.

A. Scalability of Singularity Loci and Workspace of 3-RPR Parallel Mechanisms

Major deterrents to the widespread of parallel mechanisms in the industrial context are a limited workspace and the presence of singular configurations within the workspace. In singular configurations, the mechanisms gain one or more degrees of freedom and consequently lose their inherent rigidity. Mathematically, a parallel mechanism exhibits a singularity when $\mathbf{J}$ becomes rank deficient and this can happen when its determinant goes to zero, $\det(\mathbf{J}) = 0$. The determinant of the Jacobian matrix of a scaled 3-RPR parallel mechanism can be simplified as follows:

$$l\, \det(\mathbf{J}_s) = \det(\mathbf{J}) \tag{6}$$

From the above, it is straightforward to deduce the scalability of the singularity locus. Moreover, from a geometric stand point, it is evident that a 3-RPR parallel mechanism preserves its workspace optimality upon applying an overall scale to the mechanism. Figure 2 illustrates the constant-orientation workspace [1], shaded area, and the singularity locus, solid circle [13], of a 3-RPR parallel mechanism for a given orientation. The vertex space of each limb is a ring centred at $\mathbf{a}_i + \mathbf{s}_i$, where $\mathbf{a}_i$ is the position vector of point A_i, with $\rho_{\min}$ and $\rho_{\max}$ as the radii for internal circle and external circle, respectively. In this paper, it is assumed that all the prismatic actuators have similar stroke defined by $\rho_{\min}$ and $\rho_{\max}$. As the constant-orientation workspace is the common area of the vertex spaces generated by each limb, an optimized mechanism with only optimal workspace as the optimization objective is a mechanism whose vertex spaces are lying completely on each other. This happens instantaneously for $\phi = 0$ and when

[1] Constant orientation workspace is the set of all possible locations of a given point of the mobile platform that can be reached for a prescribed orientation.

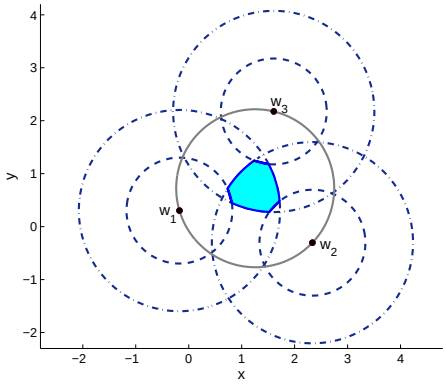

Fig. 2. Mechanism workspace for $\lambda_a = 1.45, \lambda_b = .35$, and $\phi = \pi/2$. Dash and dash-dot circles (with $\rho_{\min}$ and $\rho_{\max}$, respectively) show the limbs' vertex spaces and the solid circle is the singularity locus.

the base and mobile platform of the mechanism are identical triangles, although this mechanism is singular for all positions of its moving platform when $\phi = 0$, i.e., an architecturally singular mechanism.

B. *Preliminary Investigation of the Mechanism Architecture*

In [13], an algebraic expression for the singularity locus of a planar 3-RPR parallel mechanism with similar base and platform is obtained which consists of a circle passing through the centres of the three rings generated by the vertex spaces, Fig. 2. Moreover, in [11] the question of scalability for a optimal 3-RPR parallel mechanism is formulated as follows which is the central idea to launch our optimization procedure: *The maximal singularity-free workspace for a 3-RPR parallel mechanism is possible for a design having equilateral triangle base (with unit area) and mobile platform and for a special ratio of link lengths of base and mobile platform.* Henceforth, in this paper, a 3-RPR parallel mechanism with equilateral triangle for the base and mobile platform is considered since it inherently adopts some optimality for its singularity and workspace. The aforementioned link lengths are λ_a and λ_b which are respectively the radius of the base and the mobile platform, Fig. 1.

IV. Kinetostatic Performance Indices

The analysis of the performance sensitivity to uncertainties is an important task [14]. The quantification of performance sensitivity, has attracted a lot of interest and many indices are proposed, such as manipulability and dexterity. As mentioned above, the most notorious indices, which are manipulability and dexterity, still entail some drawbacks [2–4] and the results obtained using them may be questioned. Therefore, in our optimization objectives these two indices are not taken into account. Here, we close the discussion about these two indices by only reviewing their scalability. The manipulability and dexterity can be formulated as follows:

$$\mu \equiv \sqrt{\det(\mathbf{J}^T\mathbf{J})}, \qquad \kappa = \| \mathbf{J} \| \| \mathbf{J}^{\dagger} \| \tag{7}$$

Geometrically, the manipulability is, up to a proportionality constant, the volume of the manipulability ellipsoid (which is the generalized Cartesian error ellipsoid resulting from the hyper-sphere in the joint error space). It should be noted that for a given scale, l, of the mechanism the manipulability, μ, would change, however optimal parameters would not be affected because the value of μ changes linearly and uniformly with l for all different values of optimization parameters. On the other hand, dexterity can be regarded as the condition number of the Jacobian matrix and provides an upper bound (and a lower bound) for the relative-error amplification. The dexterity index does not apply to dimensionally non homogeneous Jacobian matrices. To circumvent this problem, homogeneous Jacobian matrices have been proposed [4, 15–17]. It should be noted that the condition number of these homogeneous Jacobians result in scale invariant objectives.

A. *Kinematic Sensitivity*

Kinematic sensitivity is defined as the maximum rotation sensitivity and the maximum point displacement sensitivity. These two indices provide tight upper bound to the end-effector rotation and point-displacement sensitivity under a unit magnitude array of actuated-joint displacements. The maximum magnitude rotation and point displacement under a unit q-norm actuator displacement are respectively:

$$\sigma_{r,q} \equiv \max_{\|\rho\|_q=1} \| \phi \|, \qquad \sigma_{p,q} \equiv \max_{\|\rho\|_q=1} \| p \| \tag{8}$$

These two indices provide separately upper bounds on the amplitude of rotation and operating-point displacement induced by a constant overall magnitude of the active-joint displacements. Thus they are referred to as the maximum rotation and point-displacement sensitivities, respectively. These pieces of information are thought to be meaningful for optimal design and have been proposed recently in [3]. Directly, from [3], it follows that the 2-norm of the above equations are:

$$\sigma_{r,2} = \frac{1}{\sqrt{\min_{i=1,2,3} \lambda_{rp,i}}} = \sqrt{\| (\mathbf{J}_r^T\mathbf{P}_p\mathbf{J}_r)^{-1} \|_2} \tag{9}$$

where $\lambda_{rp,i}$, $i = 1, 2, 3$ are the eigenvalues of $\mathbf{J}_r^T\mathbf{P}_p\mathbf{J}_r$ and $\mathbf{P}_p$ is:

$$\mathbf{P}_p \equiv \mathbf{I}_{3\times 3} - \mathbf{J}_p(\mathbf{J}_p^T\mathbf{J}_p)^{-1}\mathbf{J}_p^T \tag{10}$$

and

$$\sigma_{p,2} = \frac{1}{\sqrt{\min_{i=1,2,3} \lambda_{pr,i}}} = \sqrt{\| (\mathbf{J}_p^T\mathbf{P}_r\mathbf{J}_p)^{-1} \|_2} \tag{11}$$

where $\lambda_{pr,i}$, $i = 1, 2, 3$, are the eigenvalues of $\mathbf{J}_p^T \mathbf{P}_r \mathbf{J}_p$ and $\mathbf{P}_r$ is:

$$\mathbf{P}_r \equiv \mathbf{I}_{3\times 3} - \mathbf{J}_r (\mathbf{J}_r^T \mathbf{J}_r)^{-1} \mathbf{J}_r^T \tag{12}$$

From the above it follows that since $\mathbf{J}_p$ is independent from the scale factor, l, consequently, the corresponding sensitivity index, i.e., the point-displacement sensitivity $\sigma_{p,2}$, becomes invariant to the scale factor, which is suitable for our optimization analysis. However, $\mathbf{J}_r$ and $\sigma_{r,2}$ are related to the scale factor l as follows:

$$\mathbf{J}_r = l\mathbf{J}_{r_o}, \qquad \sigma_{r,2} = \frac{\sigma_{r,2_{l=1}}}{l} \tag{13}$$

Since $\sigma_{r,2}$ changes linearly and uniformly by $\frac{1}{l}$ for all different value of optimization parameters, thus upon changing the scale factor, l, the optimal parameters remain unaffected. Since the kinetostatic indices are, in general, dependent on the pose of the mobile platform, thus the next step consists in extending these two indices to all poses which the mechanism can reach. Following the reasoning presented in [18], instead of considering the index I for a specific pose, a global index ζ_I is introduced over the manipulator workspace W by:

$$\zeta_I = \frac{\int_W I dW}{\int_W dW} \tag{14}$$

One should be aware that ζ_I tends to infinity at singular poses when it is applied for $\sigma_{p,2}$ and $\sigma_{r,2}$. Therefore it is unable to distinguish mechanisms which have singular poses in their workspace. In the case that the dimensional synthesis inherently removes singular poses, then Eq. (14) holds for the entire workspace. However, in general, cleaning the whole workspace from all singular poses directly from the initial dimensional synthesis is often impossible and, consequently, the kinematic sensitivity performance indices in Eq. (14) must be defined accordingly. To circumvent this problem the reasoning applied to the condition number in [18] is considered. Point displacement and rotation sensitivities are bounded from zero to infinity and hence their inverses are not more helpful in the same interval. As the minimization of these indices is of interest, the maximization of the inverse of their offshoot is suggested. Consequently, Eqs. (11) and (9) are reformulated as follows to be applicable to our optimization purpose:

$$\sigma'_{r,2} = \frac{1}{1+\sigma_{r,2}}, \qquad \sigma'_{p,2} = \frac{1}{1+\sigma_{p,2}}. \tag{15}$$

We then have:

$$0 > \sigma'_{r,2},\, \sigma'_{p,2} > 1 \tag{16}$$

B. Mechanism Stiffness

Although the stiffness of a mechanism is not a kinematic property per se, the reason which encourages us to consider it besides our kinematic optimization objectives is to have a better insight about the relation between the two recent kinematic sensitivity indices and the stiffness of the mechanism under study. In short, stiffness is the measured ability of a body or structure to resist deformation due to the action of external forces. More specifically, the stiffness of a parallel mechanism at a given point in its workspace can be characterized by its stiffness matrix which relates the forces and torques applied at the gripper link in Cartesian space to the corresponding linear and angular Cartesian displacements. The stiffness matrix of the mechanism in Cartesian space is then given by the following expression:

$$\mathbf{K}_c = \mathbf{J}^T \mathbf{K}_J \mathbf{J} \tag{17}$$

In the above, $\mathbf{K}_J$ is the joint stiffness matrix of the parallel mechanism. Specifically, $\mathbf{K}_J = \text{diag}[k_1, k_2, k_3]$, where each of the actuator in the parallel mechanism is modelled as an elastic component. Furthermore, k_i is a scalar representing the joint stiffness of each actuator, which is modelled as a linear spring. In the case for which all the actuators have the same stiffness, $k = k_1 = k_2 = k_3$, then Eq. (17) reduces to:

$$\mathbf{K}_c = k\mathbf{J}^T \mathbf{J} \tag{18}$$

Moreover, the diagonal components of the stiffness matrix are used as the system stiffness value. These components represent the pure stiffness in each direction—in our case, the translation along the x and y axes and the rotation around the z axis— as well as reflecting the rigidity of machine tools more clearly and concisely. Hence considering the consistency of the units, two objective functions could be defined for the stiffness optimization:

$$S_r = K_{c_{33}} \tag{19}$$

$$S_t = \eta_1 K_{c_{11}} + \eta_2 K_{c_{22}} \tag{20}$$

In the above, S_r and S_t could be considered respectively as the mechanism rotational and translational stiffness. Relations, for $i = 1, 2, 3$, $K_{c_{ii}}$ represents the diagonal components of the stiffness matrix of the mechanism and η_i is the weight factor for each directional stiffness characterizing the priority of the stiffness in this direction. Equations (19) and (20) can be rewritten as follows:

$$S_r = kl^2 \sum_{i=1}^{3} J_{ri}^2 \tag{21}$$

$$S_t = k(\eta_1 \sum_{i=1}^{3} n_{i_x}^2 + \eta_2 \sum_{i=1}^{3} n_{i_y}^2) \tag{22}$$

Equation (21) shows that the mechanism rotational stiffness is a linear function of the mechanism scale, and as pointed out for the manipulability index, μ , and the kinematic rotational sensitivity, $\sigma_{r,2}$, this factor changes the value of mechanism rotational stiffness. However, for a given scale

of the mechanism, the optimal design parameters do not change.

Equation (22) contains only unit vectors, thus this objective is independent from mechanism scale where η_1 and η_2 stand for the stiffness priorities along the x and y axes, respectively. Usually, the task to be performed by the manipulators are unknown and unpredictable where the uncertainty is prominently present. Hence, there should not be any preferred general orientation for which the manipulator should exhibit better performances and accordingly in [19] the symmetry for a 3-RPR parallel mechanism is considered. By symmetry, the actuators are assumed identical, i.e., $k = k_1 = k_2 = k_3$, and there is no priority direction for the stiffness ($\eta_1 = \eta_2 = 1$). As $n_{i_x}^2 + n_{i_y}^2 = 1$ for $i = 1, 2, 3$, this assumption results in a constant value of magnitude 3 for the translational stiffness of the mechanism for different poses of the mechanism and, therefore, S_t is excluded from the optimization objectives.

V. Optimization Procedures

In what follows for this section, first the optimization parameters, λ_a and λ_b, are refined, by addressing their roles in normalization, existence of the nonvanishing singularity-free workspace and maximization of the global singularity-free workspace. Then the single and multi optimization procedures are presented, including the final results for the optimized 3-RPR parallel mechanism.

A. Normalization According to Scalability

According to the scalability of the parallel mechanism under study, it is proper to set up the optimization based on the unit length of its actuators. Due to the scale invariance of the optimality of the mechanism under study, the optimization can be implemented by considering $l = 1$, and the obtained optimal mechanism can be modified according to the desired workspace volume. This means that the optimization results in an identity between the length of actuators and the size of workspace and this should be consistent with the actuators strokes. To do so, in this paper, it is assumed that the strokes of actuators range from 0.9 to 1.9 of their initial leg length which implies that:

$$\rho_{\min} = l, \qquad \rho_{\max} = 1.9\, l \tag{23}$$

To have a mechanism of practical interest, the mobile platform which carries the manipulator tool must be constrained in order to have a reasonable size. As the scale of the mechanism is approximately proportional to the instrument that is used by its mobile platform, the constraint is adopted as a linear function of robot scale such that:

$$\lambda_b \geq 0.2\, l \tag{24}$$

This constraint determines a half plane for choosing λ_a and λ_b, Fig. 3.

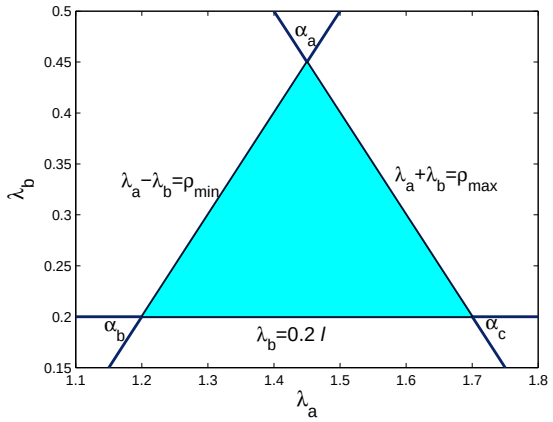

Fig. 3. Constraints and design space of λ_a, λ_b.

B. Existence of a Nonvanishing Singularity-free Workspace for All Orientation

In order to have a mechanism of practical interest, the optimization parameters, λ_a and λ_b, should be arranged in such way that the optimization procedure ends up with a nonvanishing workspace for every angle ϕ. Moreover, in general, the limited workspace of parallel mechanisms which is also segmented by singularities, makes the trajectory planning of parallel mechanisms a delicate task, thereby justifying the maximal singularity-free workspace analysis. This channels us to address the existence of a nonvanishing singularity-free workspace for every orientation of the mechanism under study. Refering to Fig. (2), coordinates of the centre of each vertex space, $\mathbf{w}_i = [w_{ix},\, w_{iy}]^T$, for different orientations of the moving platform could be formulated as follows:

$$\mathbf{w}_i = \mathbf{a}_i - \mathbf{Q}\mathbf{b'}_i \tag{25}$$

For this particular design with equilateral triangle for the base and mobile platform, the centres of three circles of vertex spaces lie exactly on the singularity circle, Fig. 2. The above leads to obtain explicitly the coordinate, $\mathbf{w}_s = [w_x,\, w_y]^T$ and radius, ρ_s, of the singularity-free workspace as follows:

$$w_x = \frac{w_{1x} + w_{2x} + w_{3x}}{3}, \qquad w_y = \frac{w_{1y} + w_{2y} + w_{3y}}{3} \tag{26}$$

$$\rho_s = \sqrt{(w_{ix} - w_x)^2 + (w_{iy} - w_y)^2} \tag{27}$$

For $\phi = 0$ and $\phi = \pi$ nonvanishing singularity-free workspace can be achieved by imposing the following constraints:

$$\lambda_a - \lambda_b > \rho_{\min}, \qquad \lambda_a + \lambda_b < \rho_{\max} \tag{28}$$

In the above, from Eq. (23), since $\rho_{\min}$ and $\rho_{\max}$ are scaled then the above constraints are not destroying the scalability

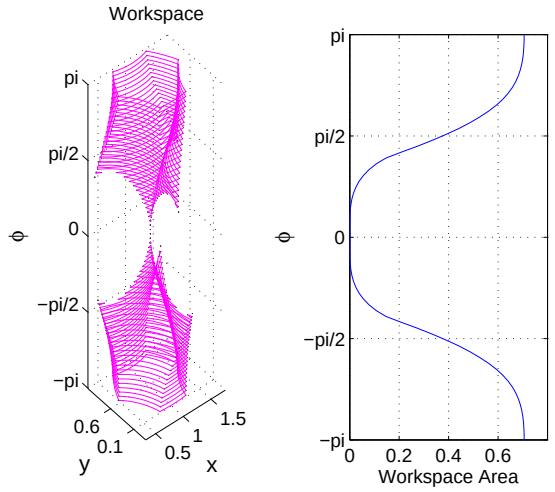

Fig. 4. Workspace as a function of ϕ for (λ_a, λ_b) sets which are located in constraint $\lambda_a - \lambda_b = \rho_{\min}$ (vertex α_b).

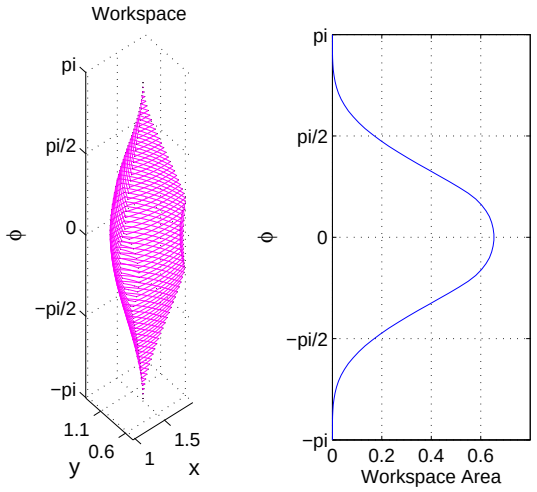

Fig. 5. Workspace as a function of ϕ for (λ_a, λ_b) sets which are located in constraint $\lambda_a + \lambda_b = \rho_{\max}$ (vertex α_c).

of the problem. As illustrated in Fig. 3, these two constraints determine the half planes which bound λ_a and λ_b. Upon considering the constraint imposed by the dimension of the platform, it can be concluded that the permitted set of values for λ_a and λ_b are inside a triangle which is defined by Eqs. (24) and (28), Fig.3. Referring to Fig. 3, points lying on the two boundary lines $\lambda_a - \lambda_b = \rho_{\min}$ and $\lambda_a + \lambda_b = \rho_{\max}$, denoted as α_a, α_b and α_c, have respectively zero workspace area for $\phi = 0$ and $\phi = \pm\pi$. Therefore, the intersection of the two boundary lines, the point denoted by α_a, results in a zero workspace area for $\phi = \{0, \pm\pi\}$.

C. Maximization of the Global Singularity-free Workspace

The global workspace of the mechanism can be regarded as 3-dimensional space for (x, y, ϕ), as shown in Fig. 4 and 5. These figures are obtained by incrementing ϕ and calculating the corresponding workspace in the (x, y) plane, for every angle ϕ. The volume of the workspace can be approximated numerically using discrete integration over ϕ using the following formulation:

$$W = \int_{-\pi}^{\pi} A(\phi) d\phi \tag{29}$$

where $A(\phi)$ is the area of workspace for a given orientation of the mobile platform, ϕ. The area of the workspace for each orientation, $A(\phi)$, can be computed by applying an integration on the boundary using Gauss Divergence theorem as proposed in [19]. However, as other mechanism performance indices should be computed using Eq. (29), the IKP is considered here to obtain the workspace. For each pose in the space, (x, y, ϕ), if the IKP verifies the stroke of all limbs ($\rho_{min} < \rho_i < \rho_{max}$, for $i = 1, 2, 3$), this pose belongs to workspace. To decrease the computational burden of this problem, an estimation of the area which is likely to be a part of workspace is helpful. For each vertex space a square shape area can be defined as follows:

$$\lim_{\min i} x : w_{ix} - \rho_{\max} < x < w_{ix} + \rho_{max} : \lim_{\max i} x \tag{30}$$

$$\lim_{\min i} y : w_{iy} - \rho_{\max} < y < w_{iy} + \rho_{\max} : \lim_{\max i} y : \tag{31}$$

Thus, conditions for the existence of all vertex spaces can be formulated as follows:

$$\max\{\lim_{\min i} x\} < x < \min\{\lim_{\max i} x\}, \quad i = 1, 2, 3 \tag{32}$$

$$\max\{\lim_{\min i} y\} < y < \min\{\lim_{\max i} y\}, \quad i = 1, 2, 3 \tag{33}$$

In order to compute the global mechanism performance indices, Eq. (14), the value of local performance indices in the workspace nodes should be accumulated and divided by the total number of workspace nodes.

D. Single Objective Optimization Using Differential Evolution

Usually in EA algorithms, variation from one generation to the next is achieved by applying crossover and/or mutation operators. In DE, mutation is applied first to generate a trial vector, which is then used within the crossover operator to produce one offspring. The DE mutation operator produces a trial vector for each individual of the current population by mutating a target vector with a weighted differential. This trial vector will then be used by the crossover operator to produce offspring. For each parent, $\mathbf{x}_i(t)$, first the trial vector should be generated, $\mathbf{u}_i(t)$, as follows: Select a target vector, $\mathbf{x}_{i1}(t)$, from the population. Then, randomly select two individuals, $\mathbf{x}_{i2}$ and $\mathbf{x}_{i3}$, from the population:

$$\mathbf{u}_i(t) = \mathbf{x}_{i1}(t) + \beta(\mathbf{x}_{i2}(t) - \mathbf{x}_{i3}(t)) \tag{34}$$

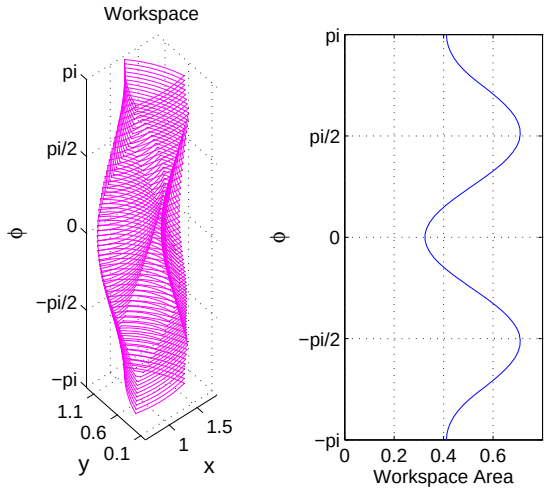

Fig. 6. Workspace as a function of ϕ for the mechanism with optimal workspace.

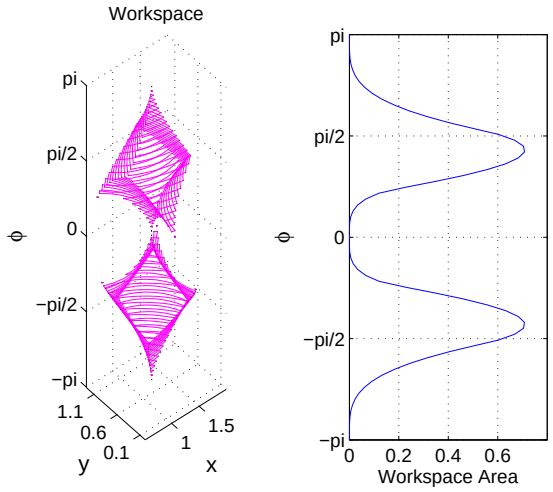

Fig. 7. Workspace as a function of ϕ for the mechanism with optimal rotational stiffness and rotation sensitivity (vertex α_a).

Objective→ Performance↓	Workspace	$\sigma_{r,2}$	$\sigma_{p,2}$	S_r
λ_a	1.4	1.45	1.45	1.45
λ_b	0.2	0.45	0.39	0.45
Workspace	3.39	1.45	1.71	1.45
$\sigma_{r,2}$	1.23	1.68	1.57	1.68
$\sigma_{p,2}$	2.05	2.08	2.09	2.08
S_r	0.07	0.5	0.35	0.5

TABLE I. Results of single objective optimization of mentioned mechanism performance indices

where $\beta\epsilon(0,\infty)$ is the scale factor, controlling the amplification of the differential variation. The DE crossover operator implements a discrete recombination of the trial vector, $\mathbf{u}_i(t)$, and the parent vector, $\mathbf{x}_i(t)$, to produce offspring, $\mathbf{x'}_i(t)$. Binomial crossover and exponential crossover are typical crossover methods, in which, some genes of the parent vector would change by the genes of trial vector to produce the offspring. To determine which individuals will take part in the mutation operation to produce a trial vector, and to determine which of the parent or the offspring will survive to the next generation, a selection function is used. Random selection is usually used to select the individuals from which difference vectors are calculated. For most DE implementations the target vector is either randomly selected or the best individual is selected. To construct the population for the next generation, deterministic selection is used, in which the offspring replaces the parent if the fitness of the offspring is better than its parent; otherwise the parent survives to the next generation. This ensures that the average fitness of the population does not deteriorate. In this paper, DE with (random) best population chromosome as target vector and binary crossover is used to find the parameters of optimal mechanism [8]. Table I represents the results of single objective optimization for the performance criteria which was described in the previous sections. As it can be observed from Table I, λ_b finds its minimum value which is 0.2 for the optimal workspace. This is consistent with Eq. (25) where the minimum leg length of vector $\mathbf{b'}_i$, which is related to λ_b, results in three vertex spaces which becomes closest as possible to each other and this for all possible orientation of the mobile platform. From Fig. 3, it can be deduced that when $\lambda_b = 0.2$, then $\lambda_a \in [1.2, 1.7]$ and the mean values is 1.45. From Table I it follows that λ_a approximately falls into its mean value ($\lambda_a = 1.4$). This can be justified by the fact that the boundary lines presented in Fig. 3, Eq. (28), are lines which workspace in their neighbourhood tends to zero (near planes $\phi \in \{0, \pm\pi\}$) and away from them, results in a larger global workspace, Fig. 6. Thus the optimization procedure attempts to avoid them and it seems that the mean value for λ_a is the optimal solution.

In addition, having in mind that a 3-RPR with equilateral triangular base and mobile platform is singular in all positions when the orientation of the platform becomes $\phi \in \{0, \pm\pi\}$ and consequently $\sigma'_{r,2}$, $\sigma'_{p,2}$ and S_r have zero value in these postures, and also close to these postures they are approximately zero. Thus the best solution found by the optimization for λ_a and λ_b is close to the vertex point α_a, since in α_a and also in its neighbourhood the workspace in singular postures tends to zero. When the orientation of the platform approaches to $\phi \in \{0, \pm\pi\}$ the workspace is nearly zero and this results in a larger mean value for $\sigma'_{r,2}$, $\sigma'_{p,2}$ and S_r which is the main purpose of applying single objective optimization to them. Figure 7 shows the workspace in (x, y, ϕ) space and the area of the workspace for different ϕ, $A(\phi)$, for α_a which is the optimal point in optimizing mechanism for $\sigma'_{r,2}$ and S_r.

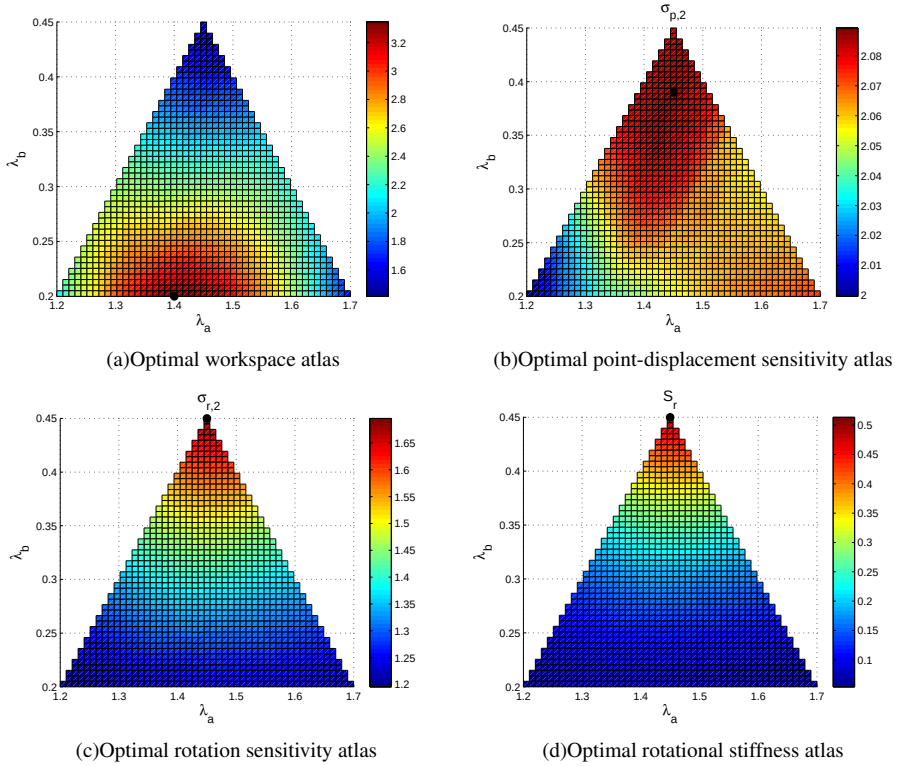

(a)Optimal workspace atlas

(b)Optimal point-displacement sensitivity atlas

(c)Optimal rotation sensitivity atlas

(d)Optimal rotational stiffness atlas

Fig. 8. Atlas representation for the results obtained form the single-objective optimization. The black marker • stands for the optimum value.

E. Multi-Objective Optimization Using NSGA-II

Multi-objective optimization is the problem of simultaneously optimizing two or more conflicting objectives with specific constraints. Here, Pareto-based multi-objective approach is used to address the issue. Mathematically, the multi-objective problem can be formulated as:

$$\begin{aligned} &\min_{\mathbf{x}} \left[\mu_1(\mathbf{x}), \mu_2(\mathbf{x}), \ldots, \mu_n(\mathbf{x})\right]^T \\ &s.t. \\ &g(\mathbf{x}) \leq 0, \quad h(\mathbf{x}) = 0, \quad x_l \leq x \leq x_u \end{aligned} \tag{35}$$

here μ_i is the i^{th} objective function, g and h are the inequality and equality constraints, respectively, and $\mathbf{x}$ is the vector of optimization or decision variables. The solution to this problem is a set of Pareto points for which improvement in one objective can only take place with the worsening of at least another objective.

EA are well-known methods in multi-objective optimization (MOEA). Genetic algorithms such as NSGA-II and strength Pareto evolutionary approach 2 (SPEA-2) are common methods. The objective approach of solving multi-objective problems needs a Pareto-compliant ranking method, favouring non-dominated solutions. In a problem with more than one objective function there are two possibilities for any two solutions $\mathbf{x}_1$ and $\mathbf{x}_2$: one dominates the other or none dominates the other. If both the following conditions hold a solution $\mathbf{x}_1$ dominates $\mathbf{x}_2$: (i) the solution $\mathbf{x}_1$ is not worse than $\mathbf{x}_2$ among all objectives and (ii) is strictly better than $\mathbf{x}_2$ in at least one objective. The Following explains a step-by-step approach for NSGA-II [10].

- Combine parent and offspring populations and construct $R_t = P_t \cup Q_t$. Do non-dominate sorting to R_t and identify different fronts: $F_i, i = 1, 2, \ldots$.
- Set new population $P_{t+1} = 0$. Set a counter $i = 1$. Until $|P_{t+1}| + F_i < N$ (N is size of P_t) perform $P_{t+1} = P_{t+1} + F_i$ and $i = i + 1$.
- If $|P_{t+1}| + F_i > N$, perform the crowding-sort procedure and include the most widely spread $(N - |P_{t+1}|)$ solutions using the crowding distance value in sorted F_i to P_{t+1}.
- Create offspring Q_{t+1} from P_{t+1} by using crossover and mutation operators.

In multi objective optimization, the number of objectives is not limited, but when is less than three, the results for the optimal Pareto could be depicted graphically which helps to investigate the objective space better. For instance, in our case, atlas maps for workspace optimization, Fig. 8(a), in comparison to other objectives, exhibits a completely different region of design space for optimality of the mechanism. As it can be deduced from atlas maps of $\sigma_{r,2}$, Fig. 8(c) and $\S_r$, Fig. 8(d), optimality patterns for selecting λ_a and λ_b are very similar. In addition, as it is a result of single objective optimization, $\sigma'_{r,2}$ and S_r, specify identical sets of (λ_a, λ_b) for optimality of the mechanism. Thus in order to have a visual conception of optimal Pareto, the mech-

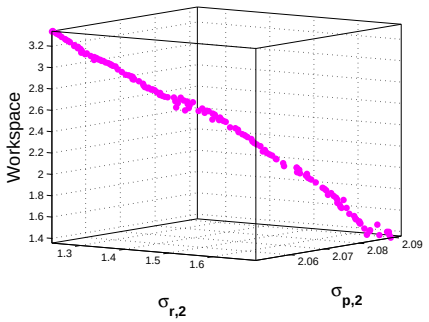

Fig. 9. Pareto front according to multi-objective optimization of the workspace, $\sigma_{r,2}$ and $\sigma_{p,2}$.

anism stiffness was not used in Pareto-based multi objective optimization. After optimization, all possible solutions in the entire solution space are obtained without the need for combining all objective functions into one. Figure 9 shows for the results of Pareto-optimal, where one can readily determine the final solutions depending on their preferences. It should be noted that for each of the Pareto points, an identity could be found between the minimum length of actuator and the size of obtained workspace. Choosing the Pareto point could be done based on the expected workspace which we expect to obtain using unit length of actuator ($l = 1$). The chosen optimal point according to this assumption from *optimal Pareto*, also results in optimal value for other two objectives. Then using the mentioned identity, for a given desired workspace the required length of actuator (and in fact the needed size of mechanism) could be obtained.

VI. Conclusion

This paper investigated the optimization of the 3-RPR parallel mechanism by the means of single and multi-objective optimization concepts. Different optimization criteria were addressed and according to the scale invariance property of some kinematic properties, workspace and singularity, it was recommended that all kinetostatic performance indices should be scale invariant. Kinematic sensitivity, rotation and point-displacement sensitivity, and stiffness are considered as kinetostatic performance. Their scalability was examined and it was revealed that both indices are scalable. As kinematic sensitivity has been proposed recently, more emphasis is place on how it should be considered in an optimization procedure. According to the optimization procedure, design parameters reduced to specifying the radii of base and mobile platform λ_a and λ_b, respectively. The optimum parameters for each design criterion were obtained using differential evolution. Moreover a complete discussion about the obtained mechanism in each case was presented. Finally, NSGA-II was used to optimize the mechanism. Two features of the multi-objective optimization technique applied in this study were of great importance: It circumvents the problem of different objectives unit inconsistency and preserves the scale invariance property of the problem. Ongoing work includes the development of a simple guideline for the optimization of parallel mechanisms.

Acknowledgement

The authors would like to acknowledge the financial support of the Natural Sciences and Engineering Research Council of Canada (NSERC) as well as the Canada Research Chair program.

References

[1] X. Kong and C. Gosselin. *Type Synthesis of Parallel Mechanisms*. Springer Verlag, 2007.
[2] J.P. Merlet. *Parallel Robots*. Springer-Verlag New York Inc, 2006.
[3] P. Cardou, S. Bouchard, and C. Gosselin. Kinematic-Sensitivity Indices for Dimensionally Nonhomogeneous Jacobian Matrices. *Transactions on Robotics IEEE*, 26(1):166 –173, feb. 2010.
[4] A. Khan and J. Angeles. The Kinetostatic Optimization of Robotic Manipulators: The Inverse and the Direct Problems. *Journal of Mechanical Design*, 128(1):168–178, 2006.
[5] Z. Gao, D. Zhang, and Y. Ge. Design Optimization of a Spatial Six Degree-of-freedom Parallel Manipulator Based on Artificial Intelligence Approaches. *Robotics and Computer-Integrated Manufacturing*, 26(2):180 – 189, 2010.
[6] R. Storn and K. Price. Differential Evolution–A Simple and Efficient Heuristic for Global Optimization over Continuous Spaces. *Journal of global optimization*, 11(4):341–359, 1997.
[7] K.V. Price, R.M. Storn, and J.A. Lampinen. *Differential Evolution: A Practical Approach to Global Optimization*. Springer Verlag, 2005.
[8] A.P. Engelbrecht. *Computational Intelligence: An Introduction*. Wiley, 2007.
[9] K. Deb. *Multi-objective Optimization Using Evolutionary Algorithms*. Wiley, 2001.
[10] K. Deb, A. Pratap, S. Agarwal, and T. Meyarivan. A Fast and Elitist Multiobjective Genetic Algorithm: NSGA-II. *IEEE transactions on evolutionary computation*, 6(2):182–197, 2002.
[11] Q. Jiang and C.M. Gosselin. Geometric Synthesis of Planar 3-RPR Parallel Mechanisms for Singularity-free Workspace. *Transactions of the Canadian Society for Mechanical Engineering*, 33(4):667–678, 2009.
[12] J. Sefrioui and C. M. Gosselin. On the Quadratic Nature of the Singularity Curves of Planar Three-degree-of-freedom Parallel Manipulators. *Mechanism and Machine Theory*, 30(4):533–551, 1995.
[13] X. Kong and CM Gosselin. Determination of the Uniqueness Domains of 3-RPR Planar Parallel Manipulators with Similar Platforms. In *Proc. Of the 2000 ASME Design Engineering Technical conferences and Computers and Information in Engineering Conference*, pages 10–13.
[14] Binaud N., Caro S., and Philippe W. Sensitivity Comparison of Planar Parallel Manipulators. *Mechanism and Machine Theory*, 45(11):1477 – 1490, 2010.
[15] C.M. Gosselin. Dexterity Indices for Planar and Spatial Robotic Manipulators. In *IEEE International Conference on Robotics and Automation*, volume 1, pages 650 –655, may. 1990.
[16] Sung-Gaun Kim and J. Ryu. New Dimensionally Homogeneous Jacobian Matrix Formulation by Three End-effector Points for Pptimal Design of Parallel Manipulators. *Robotics and Automation, IEEE Transactions on*, 19(4):731 – 736, aug. 2003.
[17] G. Pond and J.A. Carretero. Formulating Jacobian Matrices for the Dexterity Analysis of Parallel Manipulators. *Mechanism and Machine Theory*, 41(12):1505 – 1519, 2006.
[18] C. Gosselin. *Kinematic Analysis, Optimization and Programming of Parallel Robotic Manipulators*. PhD thesis, Dept. of Mechanical Engineering, McGill, Montreal, Canada, 1989.
[19] C. Gosselin and J. Angeles. The Optimum Kinematic Design of a Planar Three-degree-of-freedom Parallel Manipulator. *J. Mech. Transm. Autom. Des.*, 110(1):35–41, 1988.